ACS APPLIED POLYMER MATERIALS

pubs.acs.org/acsapm
Article

Synergistic Combination of Cross-Linked Polymer and Concentrated Ionic Liquid for Electrolytes with High Stability in Solid-State Lithium Metal Batteries

Mingjie Zhang, Faezeh Makhlooghiazad,* Urbi Pal, Mahin Maleki, Shinji Kondou, Giuseppe Antonio Elia, Claudio Gerbaldi,* and Maria Forsyth

Cite This: ACS Appl. Polym. Mater. 2024, 6, 14469−14476
Read Online

ACCESS | Metrics & More | Article Recommendations | Supporting Information

ABSTRACT: Poly(ethylene oxide)—(PEO-based solid polymer electrolytes (SPEs) are regarded as excellent candidates for solid-state lithium metal batteries (SSLMBs) due to their inherent safety advantages, processability, low cost, and excellent Li+ ion solvation. However, they suffer from limited oxidation stability (up to 4 V vs Li^+/Li). In this study, a crosslinked polymer-in-concentrated ionic liquid (PCIL) SPE consisting of PEO, *N*-propyl-*N*-methylpyrrolidinium bis(fluorosulfonyl)imide (C_3mpyrFSI) ionic liquid (IL), and lithium bis(fluorosulfonyl)imide (LiFSI) salt is developed. The adopted UV-crosslinking strategy synergistically reduces PEO crystallinity while increasing the amount of encompassed lithium salt and IL and improves PEO oxidative stability, therefore leading to enhanced electrochemical performance. The physical and electrochemical properties of both linear and crosslinked SPEs are explored and compared. The designed cross-linked SPEs exhibited a promisingly high oxidative stability of 4.9 V vs Li^+/Li and high ambient temperature ionic conductivity of 4×10^{-4} S cm^{-1}. Stable and reversible lithium plating/stripping is demonstrated in symmetrical Li||Li cells over hundreds of hours. High-loading solid-state lithium iron phosphate (LFP)||Li cells show favorable cycling with over 90% capacity retention at 0.1C over 100 cycles at 50 °C. High voltage solid-state lithium manganese oxide (LMO)||Li cells exhibit promising cycling with a 93% capacity retention at a 0.2 C rate over 50 cycles at 50 °C. Thus, the combination of concentrated ionic liquid electrolytes in a crosslinked PEO-based matrix enables a pathway for designing high-performing SPEs for high energy density solid-state LMBs.

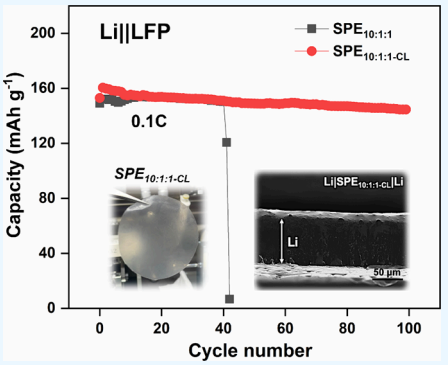

KEYWORDS: *crosslinking, electrolyte, PEO, ionic liquid, Li metal battery, solid-state battery*

1. INTRODUCTION

The pursuit of advanced energy storage technologies has significantly featured the role of lithium metal batteries (LMBs) owing to their superior energy density and potential for enabling long-range electric vehicles. However, the widespread adoption of LMBs is hindered by safety concerns related to liquid electrolytes, which are prone to flammability and stability issues. This has promoted the exploration of solid electrolytes as a safer alternative. The pioneering work of Wright and Armand in the 1970s ignited the interest and passion for research into solid polymer electrolytes (SPEs) for rechargeable solid-state batteries.[1,2] Since then, poly(ethylene oxide) (PEO) has become a frontrunner in SPEs due to its high safety, ease of processing, low cost, and good compatibility with lithium metal, making it attractive for integration into next-generation LMBs.[3,4] High molecular weight PEO offers the benefits of suppressing Li dendrite formation due to its superior mechanical properties and enhanced cycling stability compared to its lower molecular weight counterpart.[5] However, the ionic conductivity of PEO at room temperature is relatively low (up to 10^{-6} S cm^{-1}) due to its semicrystalline structure, which hinders chain mobility—critical for efficient ion transport. As a result, relatively high operating temperatures are often required for optimal performance. Additionally, PEO-based SPEs are often limited by a narrow electrochemical stability window (ESW < 4 V vs Li^+/Li) due to the low oxidative stability of ether oxygens.[1,4,5] These drawbacks considerably constrain their practical use in high voltage solid-state LMBs. To address these challenges, recent research has focused on modifying the PEO microstructure, including the addition of inorganic fillers,[6−8] plasticizing ionic liquids,[10] copolymerization,[11] and creating cross-linked PEO matrices.[9,10]

Received: August 11, 2024
Revised: November 10, 2024
Accepted: November 11, 2024
Published: December 1, 2024

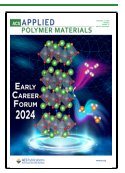

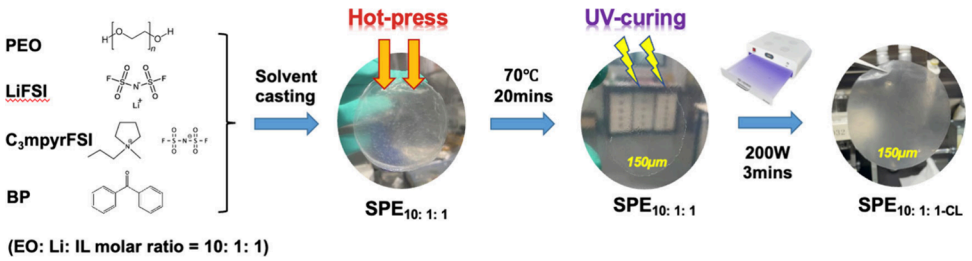

Figure 1. PCIL-SPEs (linear and cross-linked) prepared by solvent casting followed by hot-press and UV-cross-linking.

Ionic liquid (IL)-based electrolytes have gained significant interest in recent years due to their superior properties, such as low vapor pressure, nonflammability, and outstanding thermal and chemical stability.[11] Recent advancements have highlighted the role of ILs in overcoming the conductivity limitations of PEO-based SPEs. For instance, Shin et al. investigated the impact of C_3mpyrTFSI ionic liquid on the ionic conductivity of PEO-based ternary polymer electrolytes and demonstrated that the inclusion of highly conductive room temperature ILs significantly enhances ionic conductivity, surpassing the limits previously observed in IL-free electrolytes.[12] Cross-linking, as a versatile polymerization technique, is often used to improve the mechanical property and hinder polymer crystallization of plasticized SPEs.[10,13,14] This is supported by recent studies conducted by Watanabe et al., who first studied the cross-linked PEO-$LiClO_4$ systems which showed decreased PEO crystallinity by decreasing Tg from −22 to −30 °C and enhanced ionic conductivity from 10^{-9} to 10^{-5} S cm^{-1} at 30 °C compared to the linear PEO system (EO/Li mole ratio = 20).[15] Joost et al. further explored ionic mobility in cross-linked PEO-based ternary SPE systems that incorporate C_4mpyrTFSI ionic liquid with a relatively low concentration of LiTFSI (25 mol %), demonstrating a decrease of Li^+-EO interactions in the ternary system due to the additional $TFSI^-$ anions from ionic liquid that contributes to the high ionic conductivity.[16]

UV-curing with benzophenone (BP) as the photoinitiator is a well-established and facile method to obtain SPE.[17] The cross-linking process, induced by UV irradiation, helps to form a stable network that enhances the mechanical integrity of the SPE while accommodating the beneficial properties of ILs. The effectiveness of UV-induced cross-linking in the development of polymer-plasticizer-salt ternary systems was further validated by other researchers.[18−20]

In recent years, inspired by the concept of a high concentrated electrolyte in traditional liquid electrolytes,[21−23] there is growing interest in concentrated ionic liquid (CIL) electrolytes due to their advantageous properties such as expanded ESW,[24] high transference number,[25] high rate capability,[26] and enhanced cycling stability.[27] Recent work from Pal et al. identified the use of an ether-aided concentrated LiFSI-C_3mpyrFSI ionic liquid electrolyte as an effective approach to enhance ion transport and interfacial stability and support fast charging.[28−30] These findings highlight the potential of CILs to work with polymers such as PEO to create robust SPE systems that overcome the limitations of traditional PEO-based systems.

In this work, we report a UV-cross-linked polymer-in-concentrated ionic liquid (PCIL) system based on PEO, lithium bis(fluorosulfonyl)imide (LiFSI), and *N*-propyl-*N*-methylpyrrolidinium bis(fluorosulfonyl)imide (C_3mpyrFSI) ionic liquid (Li^+:IL molar ratio = 1:1). By focusing on the enhancement of ion transport, electrochemical stability, and cell performance, we seek to address a critical gap in the current understanding of PEO-based SPEs. The combination of UV cross-linking and CIL incorporation has resulted in SPEs with high ionic conductivity at ambient temperature, a wide ESW, and superior performance in solid state LMBs (SSLMBs). The obtained PCIL-SPEs demonstrate stable and reversible cycling toward Li metal electrodes, making this approach highly promising for the development of high-performance SSLMBs. Thus, by leveraging concentrated ionic liquids in conjunction with UV-cross-linking, we offer a robust approach to overcoming the limitations of conventional PEO-based SPEs, paving the way for their practical application in future advanced energy storage systems.

2. EXPERIMENTAL SECTION

2.1. Materials. Poly(ethylene oxide) (PEO, M_w 5,000,000, Sigma-Aldrich) was subjected to vacuum drying at 50 °C for 24 h before use. *N*-propyl-*N*-methylpyrrolidinium bis(fluorosulfonyl) imide (C_3mpyrFSI, purity 99.5%, Solvionic) and lithium bis(fluorosulfonyl)-imide (LiFSI, purity 99.9%, Nippon Shokubai) were subjected to vacuum drying at 50 °C for 48 h before use. Benzophenone (BP) obtained from Sigma-Aldrich was utilized without further purification for the cross-linking process. Lithium iron phosphate (LFP) was purchased from Custom Cells with an areal capacity of 1 mAh cm^{-2} and active mass loading of ∼6 mg cm^{-2}. Lithium manganese oxide (LMO) powder was provided by Calix Ltd. Carbon superP65 was obtained from Sigma-Aldrich, and polyvinylidene fluoride (PVDF) was ordered from Alfa Aesar (99.9% purity). Materials were stored in Ar-filled glove box before SPE preparation.

2.2. Solid Polymer Electrolyte Preparation. The polymer-in-concentrated ionic liquid SPEs (PCIL-SPEs) were prepared by using a solvent casting technique within an Ar-filled glovebox. The preparation steps are shown in Figure 1. First, predetermined amounts of the LiFSI salt and C_3mpyrFSI IL (Li^+:IL molar ratio = 1:1) were mixed and dissolved overnight at room temperature. Then, the obtained solutions were mixed with various amounts of PEO in acetonitrile with EO:Li^+:IL molar ratios equal to 10:1:1. The obtained solutions were then cast into silicon molds and rested for 48 h to ensure slow evaporation of the solvent. The obtained free-standing solid membranes were then sandwiched between two Mylar foils and hot-pressed (70 °C, 2 MPa for 10 min) to obtain homogeneous membranes with a thickness of 150 ± 10 μm.

Cross-linked PCIL-SPEs were then prepared by using benzophenone (BP, 5 wt % of PEO) as the photoinitiator and photopolymerised in a TBK 905 UV curing box (power 200W) for 3 min right after hot-pressing. The prepared SPEs were then transferred to a Buchi oven for a secondary vacuum drying process (50 °C for 24 h) before further characterization. All prepared SPEs were kept in an Ar-filled glovebox.

2.3. Characterization Techniques. A Mettler Toledo Differential Scanning Calorimetry (DSC) instrument was used to study the phase behavior of the designed SPEs. The measurements were

https://doi.org/10.1021/acsapm.4c02520
ACS Appl. Polym. Mater. 2024, 6, 14469−14476

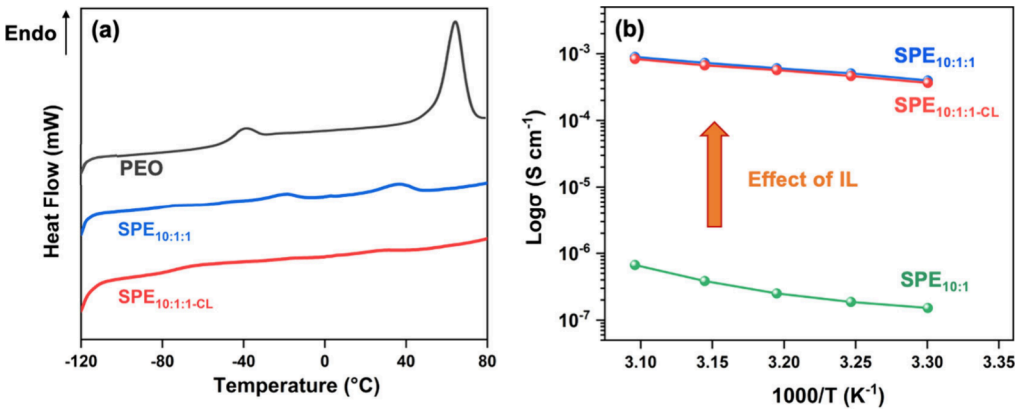

Figure 2. (a) Phase behavior of cross-linked $SPE_{10:1:1\text{-}CL}$ compared with linear $SPE_{10:1:1}$ and pure PEO. (b) Ionic conductivity of cross-linked $SPE_{10:1:1\text{-}CL}$ compared with linear $SPE_{10:1:1}$ and linear $SPE_{10:1}$ without IL.

performed over −120−80 °C at a heating/cooling rate of 10 °C min^{-1}. Sample loading was kept at approximately 10 mg.

Ionic conductivity (σ) of the designed SPEs was measured by electrochemical impedance spectroscopy (EIS) analysis (MTZ-35 impedance analyzer, Biologic). The measurements were performed over the temperature range of 30−50 °C in frequency from 0.1 Hz to 1 MHz. A SS|PCIL-SPEs|SS (stainless-steel) coin cell configuration was used. The bulk resistance was calculated from the impedance curve at high frequency, and the ionic conductivity was calculated by the equation $\sigma = l/(R_b \cdot A)$, where σ is the ionic conductivity (S cm^{-1}), R_b is the bulk resistance (derived from the impedance curve), l is the membrane thickness, and A is the area.

Raman spectra were obtained using a Renishaw Invia microscope with a laser generating 633 nm (red) light, delivering 13.0 mW at the sample. The laser power was set to 10% with the exposure time of 60 s and one accumulation. All measurements were done under room temperature in a sealed home-built sample holder with a quartz window in the range of 100 to 3200 cm^{-1}. Baseline corrections and normalization were applied to the spectra. The Voigt function was used to deconvolute bands into constituent peaks.

Thermal gravimetric analysis (TGA) was performed using a Mettler Toledo TGA STAR instrument to understand the thermal stability of the SPEs with a sample loading of 10 mg. Mass loss was recorded over 30−600 °C with a 10 °C min^{-1} heating rate under constant N_2 flow. Sample loading was kept at approximately 10 mg.

Scanning electron microscopy (SEM) analysis was carried out for the pristine SPEs as well as cycled cells. A coin cell disassembly unit (Hohsen) was used inside a glovebox to disassemble the cycled cells. The JSM-IT300 SEM from JEOL (Japan) was used to study the surface and cross-section morphology with a 10 kV acceleration voltage.

2.4. Electrode Preparation, Cell Assembly, and Electrochemical Measurements. The LMO electrode was prepared by mixing LMO powders, Super C65, and PVDF (80:10:10 wt %) in NMP. The casting and drying methods for the LMO cathodes were as previously described.[31] The resulting LMO electrodes hade a loading of 7 mg cm^{-2} and an area capacity of 1 mA cm^{-2}. On the other hand, the LFP electrodes from Custom Cells had a similar areal capacity of 1 mA cm^{-2} with ∼6 mg cm^{-2} active material loading. The electrodes were then cut into 8 mm diameter discs before the coin cell assembly.

For all the battery measurements, lithium metal (100 μm, Gelon) was used as the anode material. Battery cells were then assembled using a Li metal anode, a free-standing designed SPE membrane, and the prepared LFP/LMO cathodes.

Electrochemical measurements were performed using a multichannel potentiostat VMP3 (BioLogic) with all measurements conducted in CR2032 coin cells (Hohsen Corp.). Linear sweep voltammetry (LSV) experiments were performed using a Li|SS (stainless steel) cell at 50 °C. The scans ran from the open-circuit voltage (OCV) up to 6 V (vs Li/Li^+) at a scan rate of 0.1 mV s^{-1}. The galvanostatic cycling for Li|Li, LFP|Li, and LMO|Li cells was also carried out. Cell cycling was performed at 50 °C, with voltage limits set to 2.5−4 V vs Li^+/Li for LFP|Li cells and 3−4.3 V vs Li^+/Li for LMO|Li cells. Two formation cycles were used before long-term cycling, unless mentioned otherwise. The reproducibility of the results was checked by multiple tests.

3. RESULTS AND DISCUSSION

3.1. Properties of Designed PCIL-SPEs. Both linear and cross-linked PCIL-SPEs were synthesized from homogeneous mixtures of PEO, LiFSI, and C_3mpyrFSI (EO:Li:IL molar ratio = 10:1:1) by solvent casting and UV-cross-linking processes, namely $SPE_{10:1:1}$ and $SPE_{10:1:1\text{-}CL}$, respectively (Figure 1). Thermal gravimetric analysis (TGA) of both $SPE_{10:1:1}$ and $SPE_{10:1:1\text{-}CL}$ confirms the thermal stability up to 220 °C which is sufficiently high for the safe operation of solid-state LMBs (Figure S1, Supporting Information).

The effect of UV-cross-linking on the phase behavior, ionic conductivity, and morphology of the prepared PCIL-SPEs is shown in Figure 2 and Figure S2. As illustrated in Figure 2a, both the melting point and enthalpy decrease dramatically after introducing CIL (Li:IL molar ratio = 1:1) to PEO, with the melting transition temperature dropping from 65 °C of pure PEO to 38 °C of $SPE_{10:1:1}$, and the T_g broadens significantly, suggesting a more complex heterogeneous system.[32,33] Notably, a small peak at approximately −20 °C appears in $SPE_{10:1:1}$, attributed to a phase transition in the C_3mpyrFSI/LiFSI mixture, suggesting limits in IL solubility and potential phase separation.[34,35] Cross-linking $SPE_{10:1:1}$ to create $SPE_{10:1:1\text{-}CL}$ results in the disappearance of both the melting and phase transition peaks, with a new, pronounced T_g appearing at −74 °C. This suggests that cross-linking leads to a highly amorphous structure and enhances the uptake of IL in the PEO matrix.[10] In addition, the presence of a single T_g in the cross-linked materials indicates good miscibility between IL and the PEO matrices.[36] To summarize, cross-linking effectively hinders crystallization of PEO and PEO-LiFSI complexes and increases the IL uptake in the cross-linked network, which is crucial for achieving high ionic conductivity due to the resulting high amorphicity of the SPEs.

Figure 2b illustrates the effect of IL content and UV-cross-linking on the ionic conductivity of the prepared SPEs. Compared to systems without IL ($SPE_{10:1}$), adding IL significantly increases the ionic conductivity, with more than 3 orders of magnitude improvement from 1.5×10^{-7} S cm^{-1} for IL-free $SPE_{10:1}$ to 4×10^{-4} S cm^{-1} for $SPE_{10:1:1}$ at 30 °C, suggesting the substantial role of IL in enhancing ionic

https://doi.org/10.1021/acsapm.4c02520
ACS Appl. Polym. Mater. 2024, 6, 14469−14476

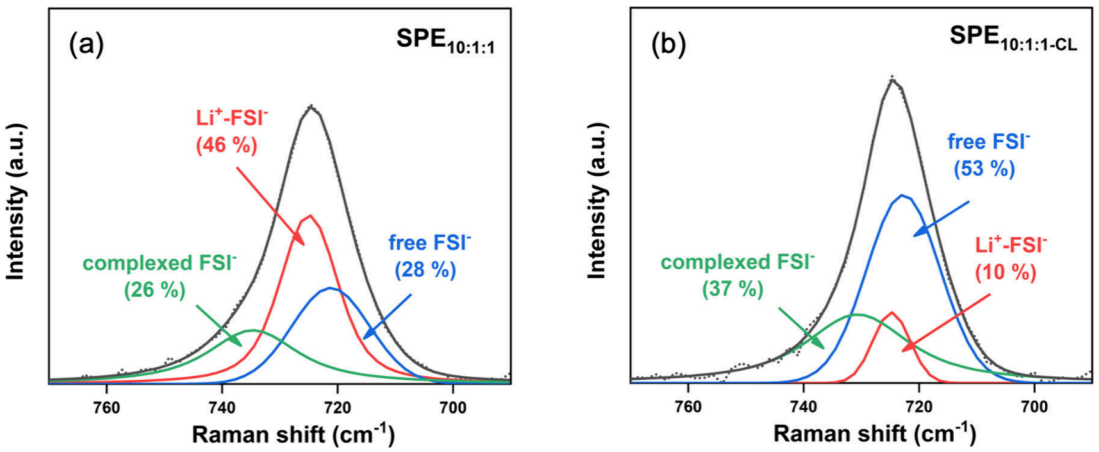

Figure 3. Raman spectra of the -SNS stretching vibration mode of FSI^- anions in (a) linear $SPE_{10:1:1}$ and (b) cross-linked $SPE_{10:1:1\text{-}CL}$. The spectra were deconvoluted to three FSI^- states, including free FSI^-, Li^+-FSI^- ion pairs, and complexed FSI^-.

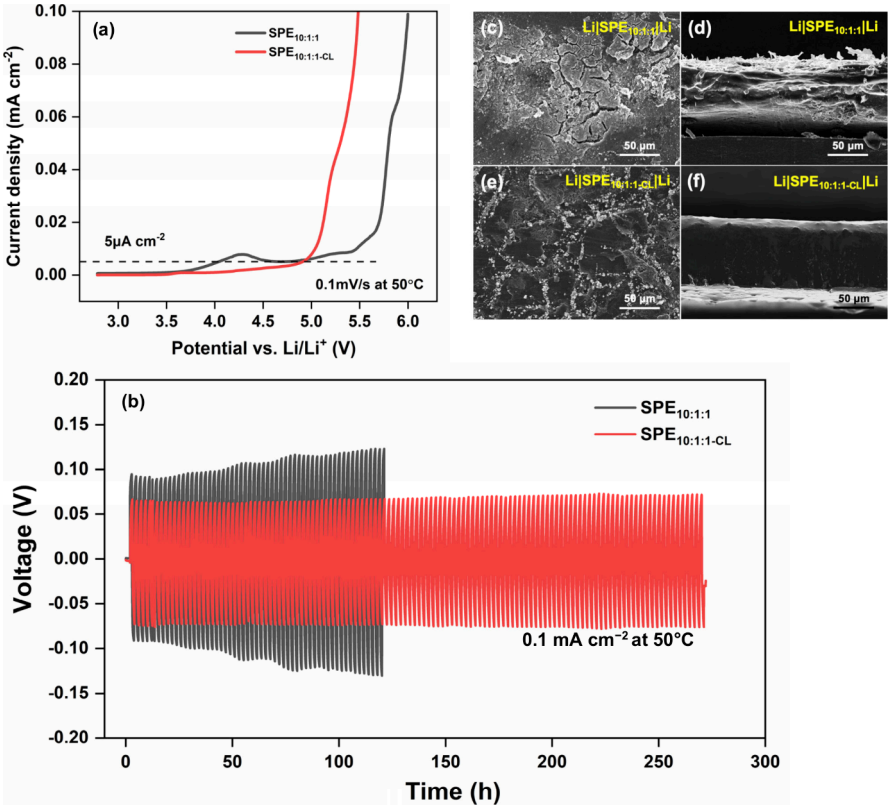

Figure 4. (a) Linear sweep voltammetry of $SPE_{10:1:1}$ and $SPE_{10:1:1\text{-}CL}$ in a Li||SS cell with a scan rate of 0.1 mV s^{-1} at 50 °C. (b) Voltage profiles of Li|$SPE_{10:1:1}$|Li and Li|$SPE_{10:1:1\text{-}CL}$|Li cells at 0.1 mA cm^{-2}. Surface (c, e) and cross-section (d, f) SEM images of Li electrodes after cycling.

conductivity. Our previous work showed that the ionic conductivity of the CIL electrolyte is 6×10^{-4} S cm^{-1} at 30 °C,[28] indicating that the ionic conductivity of the CIL electrolyte is very well maintained after mixing PEO. After cross-linking, $SPE_{10:1:1\text{-}CL}$ shows a slight decrease in conductivity, consistent with an overall high salt content system.[37] Cross-linking generally increases the formation of amorphous phases that facilitate conductivity in systems with high polymer content.[38] However, it can also restrict the polymer chain movement, hindering ion transport. This effect is particularly noticeable in systems with low polymer content that are already highly amorphous and conductive, such as $SPE_{10:1:1}$.[37] Overall, while cross-linking affects ionic conductivity by restricting chain mobility, its downside impact is mitigated by the reduced SPE crystallinity and increased IL uptake. Furthermore, the impact of cross-linking on ionic conductivity is much less pronounced compared to the influence of IL concentration.

The surface morphology of the prepared SPEs was characterized by SEM analysis, as shown in Figure S2. Compared to $SPE_{10:1:1}$, the cross-linked $SPE_{10:1:1\text{-}CL}$ shows a dense, smooth surface with a high degree of amorphous nature. The nonuniform and hardly homogeneous texture of $SPE_{10:1:1}$ transformed into a finer wrinkled feature after cross-linking, which is likely due to the increased encompassing of lithium

https://doi.org/10.1021/acsapm.4c02520
ACS Appl. Polym. Mater. 2024, 6, 14469−14476

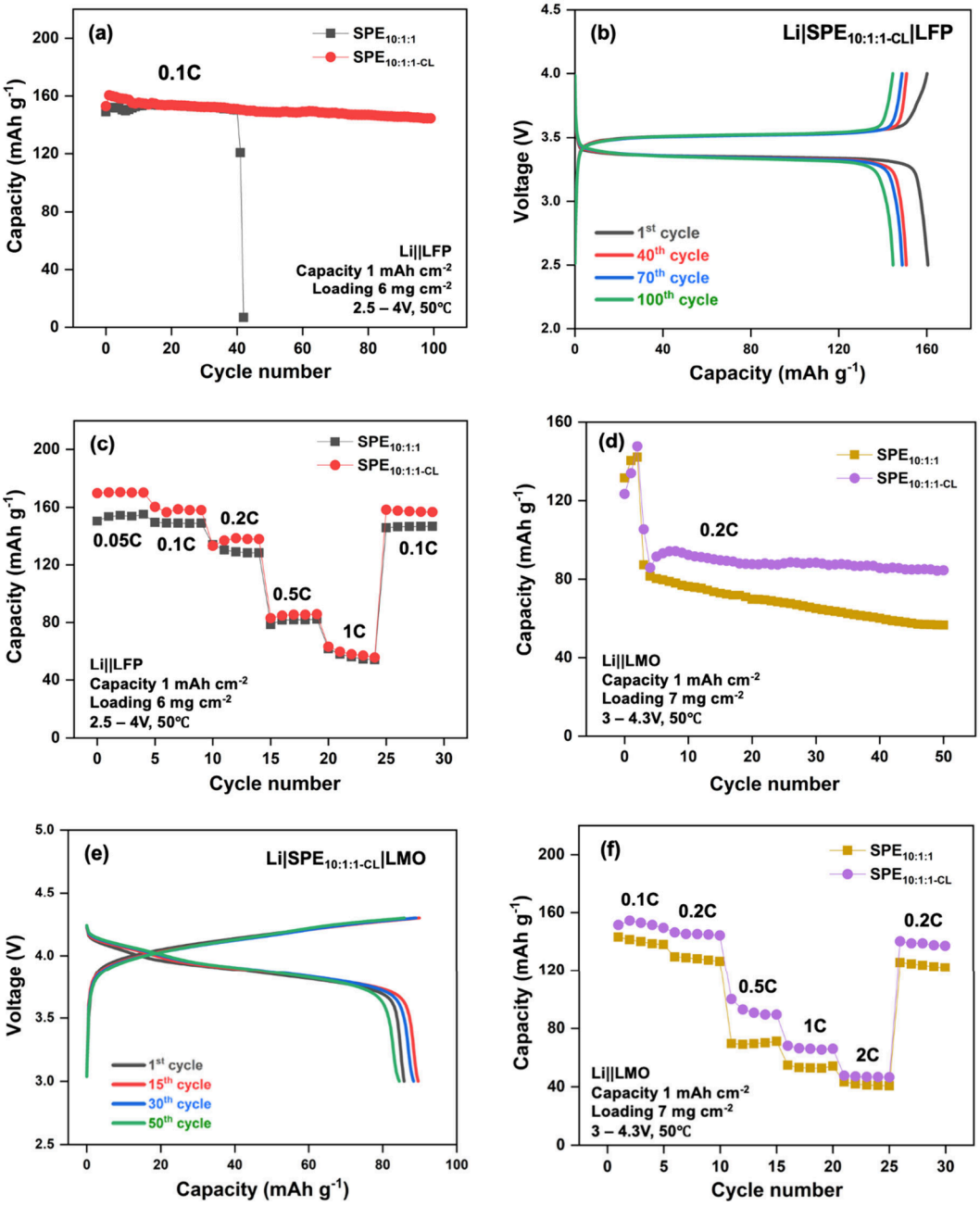

Figure 5. (a) Cycling performance of the LFP||Li (active mass loading ~6 mg cm^{-2}) cell cycled at a 0.1 C rate between 2.5−4.0 V for 100 cycles at 50 °C. (b) Charge−discharge profiles of different cycle numbers at a 0.1 C rate. (c) Rate performance of the LFP||Li cell at different C rates. (d) Cycling performance of the LMO||Li (active mass loading ~7 mg cm^{-2}) cell cycled at a 0.2 C rate between 3−4.3 V for 50 cycles at 50 °C. (e) Charge−discharge profiles of different cycle numbers at a 0.2 C rate. (f) Rate performance of the LMO||Li cell at different C rates.

salt and IL, leading to a more homogeneous and mechanically robust network.[13,39]

3.2. Raman Spectroscopy Analysis. Raman spectroscopy was performed on linear $SPE_{10:1:1}$ and cross-linked $SPE_{10:1:1-CL}$ to investigate and reveal the effect of cross-linking on cation−anion interactions by identifying the states of FSI^- in the Raman shift between 700 and 800 cm^{-1} (full Raman spectra is given in Figure S3, Supporting Information). The -SNS stretching mode of FSI^- in the PCIL-SPEs was deconvoluted into three constituent peaks: free FSI^- at 721−723 cm^{-1}, Li^+-FSI^- ion pairs at 725 cm^{-1}, and complexed FSI^- anions at 730−735 cm^{-1} (aggregated ion clusters).[40] As shown in Figure 3, the linear $SPE_{10:1:1}$ (Figure 3a) has a lower proportion of the free FSI^- state (28%) and a higher proportion of Li^+-FSI^- ion pairs (46%). In contrast, the cross-linked $SPE_{10:1:1-CL}$ (Figure 3b) has a much higher proportion of free FSI^- anions (53%) and a significantly lower amount of Li^+-FSI^- ion pairs (10%). In this system, the plasticizing effect of the concentrated IL is likely the primary driver of Li^+ solvation by weakening the strong Li-EO interactions. Cross-linking, meanwhile, reduces the crystallinity of PEO, making the polymer more homogeneously amorphous, which in turn facilitates Li^+-FSI^- ion pair dissociation.[40,41] This dissociation increases the availability of Li^+ for Li^+-EO coordination. Furthermore, the spatial segregation of PEO chains due to cross-linking likely

https://doi.org/10.1021/acsapm.4c02520
ACS Appl. Polym. Mater. 2024, 6, 14469−14476

promotes a more uniform distribution of FSI^- anions and ion clusters.[41]

The cross-linked $SPE_{10:1:1\text{-}CL}$ also exhibited a higher proportion of complexed FSI^- anions, indicating the presence of aggregated ion clusters. The cross-linked polymer network may have helped to segregate the large, aggregated domains into more uniformly distributed ion clusters to facilitate Li^+ transport.[41] Therefore, we believe that cross-linking results in enhanced Li^+-FSI^- ion pairs dissociation and more uniformly distributed ion clusters, which would account for the high ionic conductivity and the potential high electrochemical stability of the cross-linked $SPE_{10:1:1\text{-}CL}$.

3.3. Electrochemical Characterization. The electrochemical stability window (ESW) of the linear $SPE_{10:1:1}$ and cross-linked $SPE_{10:1:1\text{-}CL}$ was evaluated in a Li||SS cell by LSV measurements. As shown in Figure 4a, the linear $SPE_{10:1:1}$ begins to oxidize slowly above 4 V vs Li^+/Li, a common behavior in PEO-based SPEs. In contrast, the cross-linked $SPE_{10:1:1\text{-}CL}$ showed high electrochemical stability up to 4.9 V vs Li^+/Li (5 μA cm^{-2} current density was used as the cutoff of a current rise[42,43]). This indicates its excellent oxidation stability and suitability for use with high-energy 4 V-classs electrodes. The enhanced electrochemical stability of $SPE_{10:1:1\text{-}CL}$ can be attributed to its cross-linked network, which limits the mobility of linear EO chains and therefore reduces their likelihood of oxidation at the cathode. Furthermore, the cross-linking likely changes the coordination environment, enhancing Li^+-EO coordination and promoting the formation of FSI^--rich ion clusters around PEO chains, as evidenced by Raman analysis. These coordinated ions and surrounding ion clusters likely form a protective layer that prevents further oxidation of EO, synergistically contributing to enhanced oxidation stability.

The ability of the cross-linked $SPE_{10:1:1\text{-}CL}$ to support lithium plating-stripping was assessed using Li||Li symmetrical cells at 50 °C, with various current densities ranging from 0.05 up to 0.4 mA cm^{-2}. The cells showed overpotentials of 20 and 125 mV at 0.05 and 0.4 mA cm^{-2}, respectively. As illustrated in Figure S4, the SPE can sustain plating-stripping polarization steps throughout the entire polarization period up to 0.4 mA cm^{-2}, demonstrating stable interfacial properties, thus compatibility with the lithium metal electrodes, and good cycling performance for a solid-state polymer electrolyte.

As shown in Figure 4b, the long-term cycling of the Li|$SPE_{10:1:1\text{-}CL}$|Li cell cycled at 0.1 mA cm^{-2} for 1 h polarization demonstrated a very stable performance, maintaining an overpotential of 60 mV over 130 cycles at 50 °C with no evidence of a short circuit. This indicates that cross-linked $SPE_{10:1:1\text{-}CL}$ is highly compatible with the Li metal electrode. The interfacial resistance decreases after 130 cycles (shown in Figure S5a), suggesting the formation of an ion-conductive and stable SEI layer at the electrode/electrolyte interface. In contrast, the Li|$SPE_{10:1:1}$|Li cell exhibits a steady increase in overpotential and a short circuit after just 60 cycles. The impedance spectra also show an increase in interfacial resistance upon successive cycling, as seen in Figure S5b.

The top- and cross-sectional SEM images of the Li electrodes from both cells after cycling (Li|$SPE_{10:1:1}$|Li cell for 60 cycles, Li|$SPE_{10:1:1\text{-}CL}$|Li cell for 130 cycles) are shown in Figure 4c-f. In the Li|$SPE_{10:1:1}$|Li cell, the electrode surface shows large cracks and mossy Li formations (Figure 4c), whereas the Li|$SPE_{10:1:1\text{-}CL}$|Li cell shows a smooth and dense Li metal surface (Figure 4e), indicating a uniform Li plating-stripping process. The cross-sectional images reveal a thick layer of dendritic/dead Li at the interface of the the Li|$SPE_{10:1:1}$|Li cell (Figure 4b), in contrast to a dense and uniform interface observed in the Li|$SPE_{10:1:1\text{-}CL}$|Li cell (Figure 4f). This confirm the formation of a smooth and compact interphase and SEI layer in the cell with cross-linked $SPE_{10:1:1\text{-}CL}$, contributing to its good cycling performance. UV-cross-linking appears to play a crucial role in suppressing Li-dendrite formation and facilitating facile and reversible Li plating-stripping.[9]

3.4. Performance of Solid-State LMBs. The prepared $SPE_{10:1:1}$ and $SPE_{10:1:1\text{-}CL}$ membranes were first incorporated into high loading (6 mg cm^{-2}) LFP||Li cells to investigate their performance in solid-state LMBs. Figure 5a shows the prolonged cycling results for both LFP|$SPE_{10:1:1}$|Li and LFP|$SPE_{10:1:1\text{-}CL}$|Li cells at 0.1 C (0.05 mA cm^{-2} current density). The LFP|$SPE_{10:1:1\text{-}CL}$|Li cell incorporating a cross-linked membrane exhibits an initial discharge capacity of 160 mAh g^{-1}, maintaining 90% of its capacity after 100 cycles, achieving excellent Coulombic efficiency of nearly 99.8% throughout cycling. In contrast, the LFP|$SPE_{10:1:1}$|Li cell with a non-cross-linked membrane exhibits an initial capacity of 158 mAh g^{-1} but experienced a short circuit after 42 cycles. Figure 5b shows the charge−discharge profiles of the LFP|$SPE_{10:1:1\text{-}CL}$|Li cell at different cycle numbers, noting that while the discharge capacity decreased, the charge and discharge curves remained very stable over 100 cycles. Impedance profiles before and after cycling showed a slight increase due to the interface stability (Figure S6). A rate capability test, detailed in Figure 5c, was conducted at current densities of 0.05 to 1 mA cm^{-2} (1C equals 1 mA cm^{-2}). Compared to the LFP|$SPE_{10:1:1}$|Li cells, the LFP|$SPE_{10:1:1\text{-}CL}$|Li cells exhibited improved rate capability, maintaining nearly full capacity at 0.05C. Overall, the battery delivered high discharge capacity ranging from 170 to 59 mAh g^{-1} at 0.05 to 1C. Figure S7a presents charge−discharge profiles of the LFP|$SPE_{10:1:1\text{-}CL}$|Li cell at various C-rates within a voltage range of 2.5−4.0 V vs Li^+/Li, showing stable potential plateaus and increasing the overpotential with higher C rates. AC impedance profiles (Figure S7b) showed a steady decrease in interfacial resistance from 0.05C to 0.2C as the cross-linked membrane adapted itself with the electrode, followed by a slight increase at 0.5C and 1C rates due to interface stability. The improved rate performance and cycling stability of the LFP|$SPE_{10:1:1\text{-}CL}$|Li cell demonstrate the advantages of the cross-linked $SPE_{10:1:1\text{-}CL}$, providing superior electrochemical stability at 50 °C.

Given the high stability at anodic voltage observed from LSV tests, LMO||Li cells were explored using the cross-linked and non-cross-linked PCIL-SPEs. Figure 5d shows the cycling performance of both the LMO|$SPE_{10:1:1}$|Li and LMO|$SPE_{10:1:1\text{-}CL}$|Li cells at 0.2C (0.1 mA cm^{-2} current density) in the voltage range of 3−4.3 V vs Li^+/Li. The LMO|$SPE_{10:1:1\text{-}CL}$|Li cell with cross-linked membrane showed an initial discharge capacity of 91.4 mAh g^{-1}, maintaining 93% of its capacity after 50 cycles, whereas the LMO|$SPE_{10:1:1}$|Li cell experienced 25% discharge capacity loss after the same number of cycles. Figure 5e presents the corresponding charge−discharge profiles of the LMO|$SPE_{10:1:1\text{-}CL}$|Li cell at different cycle numbers, showing stable and relatively small overpotential throughout cycling. Figure S8 shows the AC impedance profiles for cells both before and after cycling. Both cells exhibited an increase in interfacial resistance, but the LMO cell with the cross-linked membrane demonstrated a smaller increase after cycling, which

https://doi.org/10.1021/acsapm.4c02520
ACS Appl. Polym. Mater. 2024, 6, 14469−14476

correlates with its superior cycling performance, as shown in Figure 5d. To evaluate the effect of cross-linking on fast charge/discharge capability, rate-capability tests were performed and compared across current densities from 0.05 to 1 mA cm^{-2} (shown in Figure 5f). The LMO|$SPE_{10:1:1\text{-}CL}$|Li cell exhibited a full capacity of 152 mAh g^{-1} at 0.1 mA cm^{-2} and a high capacity of 145 mAh g^{-1} at 0.1 mA cm^{-2}. The cell maintained 45 and 32% of its capacity at 1 and 2 mA cm^{-2} (2C), respectively. The current density was reduced back to 0.1 mA cm^{-2}, and the capacity was restored to 139 mAh g^{-1}. The voltage profiles of the LMO|$SPE_{10:1:1\text{-}CL}$|Li cell at different C rates are given in Figure S9.

Finally, compared with other types of PEO-based SPEs reported in the literature, the promising performances of the developed cross-linked $SPE_{10:1:1\text{-}CL}$ are highlighted (as shown in Table S1). It shows not only excellent cycling performance with high loading LFP cathodes, but also remarkably good compatibility with high loading, high energy 4 V-class LMO cathodes, which is an outstanding result within the PEO-based SPE family. Our findings collectively highlight the synergistic benefits of concentrated ionic liquid and the cross-linking approach in the designed PCIL-SPEs. The superior rate performance and prolonged cycling stability observed in the cross-linked PCIL-SPEs suggest that they are a promising avenue for their deployment in high energy density solid-state LMBs.

4. CONCLUSION

In this study, we designed cross-linked PEO-in-concentrated ionic liquid (CIL) SPEs for use in high energy solid-state LMBs. The proper combination of using CIL and UV-cross-linking shows synergistic advantages in reducing PEO crystallinity, increasing ionic conductivity, and enhancing the electrochemical stability of the newly developed SPEs. These innovations yield cross-linked $SPE_{10:1:1\text{-}CL}$ with high ambient temperature ionic conductivity of 4×10^{-4} S cm^{-1} and a wide electrochemical stability window reaching up to 4.9 V vs Li^+/Li. Raman analysis confirms that these promising properties are ascribed to enhanced Li^+ solvation and increased Li^+-EO coordination after cross-linking, which significantly enhances SPE oxidation stability. The cross-linked PCIL-SPEs demonstrated stable Li symmetric plating/stripping cycling and remarkable electrochemical performance (almost full capacity, excellent Coulombic efficiency, and stable cycling even at high current regimes) with both high loading LFP and, particularly, 4V-class LMO cathodes, highlighting their strong potential for practical applications in high energy density solid-state LMBs. This study not only advances the development of PEO-based SPEs but also enlightens their potential to impact the broader field of sustainable and high-performance energy storage solutions.

ASSOCIATED CONTENT

Supporting Information

The Supporting Information is available free of charge at https://pubs.acs.org/doi/10.1021/acsapm.4c02520.

Additional results and comparison of developed PEO-based PiCIL-SPE to PEO-based SPEs from the literature (PDF)

AUTHOR INFORMATION

Corresponding Authors

Faezeh Makhlooghiazad − *Institute for Frontier Materials (IFM), Deakin University, Burwood, Victoria 3125, Australia;* orcid.org/0000-0002-8002-9668; Email: f.makhlooghiazad@deakin.edu.au

Claudio Gerbaldi − *GAME Lab, Department of Applied Science and Technology (DISAT), Politecnico di Torino, 10129 Torino, Italy; National Reference Center for Electrochemical Energy Storage (GISEL) - INSTM, 50121 Firenze, Italy;* orcid.org/0000-0002-8084-0143; Email: claudio.gerbaldi@polito.it

Authors

Mingjie Zhang − *GAME Lab, Department of Applied Science and Technology (DISAT), Politecnico di Torino, 10129 Torino, Italy;* orcid.org/0000-0002-9661-1820

Urbi Pal − *Institute for Frontier Materials (IFM), Deakin University, Burwood, Victoria 3125, Australia*

Mahin Maleki − *Institute for Frontier Materials (IFM), Deakin University, Burwood, Victoria 3125, Australia*

Shinji Kondou − *Institute for Frontier Materials (IFM), Deakin University, Burwood, Victoria 3125, Australia;* orcid.org/0000-0002-7782-7431

Giuseppe Antonio Elia − *GAME Lab, Department of Applied Science and Technology (DISAT), Politecnico di Torino, 10129 Torino, Italy; National Reference Center for Electrochemical Energy Storage (GISEL) - INSTM, 50121 Firenze, Italy;* orcid.org/0000-0001-6790-1143

Maria Forsyth − *Institute for Frontier Materials (IFM), Deakin University, Burwood, Victoria 3125, Australia;* orcid.org/0000-0002-4273-8105

Complete contact information is available at: https://pubs.acs.org/10.1021/acsapm.4c02520

Notes

This manuscript reflects only the authors' views and opinions; neither the European Union nor the European Commission can be considered responsible for them.

The authors declare no competing financial interest.

ACKNOWLEDGMENTS

The PSIONIC project has received funding from the European Union's Horizon Europe Research and Innovation Programme under Grant Agreement N. 101069703. The authors would like to acknowledge the financial support of the European Union's Horizon 2020 research and innovation programme under the Marie Skłodowska-Curie Grant agreement (Grant No. 860403) and the Australian Research Council for providing funding through the Industry Transformation Training Centre for Future Energy Technologies (storEnergy). Deakin University's Advanced Characterisation Facility is acknowledged for use of the NMR facility. The authors also thank the Battery Technology Research and Innovation Hub (BatTRI-Hub) at Deakin University for their battery prototyping facilities. This study was carried out within the MOST−Sustainable Mobility Center, which received funding from the European Union Next- GenerationEU (PIANO NAZIONALE DI RIPRESA E RESILIENZA−PNRR−MISSIONE 4 COMPONENTE 2, INVESTIMENTO 1.4 e D.D. 1033 June 17, 2022, CN00000023).

REFERENCES

(1) Armand, M. Polymer solid electrolytes - an overview. *Solid State Ion.* **1983**, *9*−*10*, 745−754.
(2) Fenton, D. E.; Parker, J. M.; Wright, P. V. Complexes of alkali metal ions with poly(ethylene oxide). *Polymer* **1973**, *14*, 589.
(3) Xue, Z.; He, D.; Xie, X. Poly(ethylene oxide)-based electrolytes for lithium-ion batteries. *J. Mater. Chem. A* **2015**, *3*, 19218−19253.
(4) Xiao, S.; Ren, L.; Liu, W.; Zhang, L.; Wang, Q. High-voltage polymer electrolytes: Challenges and progress. *Energy Storage Mater.* **2023**, *63*, 102970.
(5) Gadjourova, Z.; Andreev, Y. G.; Tunstall, D. P.; Bruce, P. G. Ionic conductivity in crystalline polymer electrolytes. *Nature* **2001**, *412*, 520−523.
(6) Chen, L.; et al. PEO/garnet composite electrolytes for solid-state lithium batteries: From "ceramic-in-polymer" to "polymer-in-ceramic. *Nano Energy* **2018**, *46*, 176−184.
(7) Song, X.; et al. Unraveling the Synergistic Coupling Mechanism of Li^+ Transport in an "Ionogel-in-Ceramic" Hybrid Solid Electrolyte for Rechargeable Lithium Metal Battery. *Adv. Funct. Mater.* **2022**, *32*, 2108706.
(8) Zhang, X.; et al. Vertically Aligned and Continuous Nanoscale Ceramic−Polymer Interfaces in Composite Solid Polymer Electrolytes for Enhanced Ionic Conductivity. *Nano Lett.* **2018**, *18*, 3829−3838.
(9) Porcarelli, L.; Gerbaldi, C.; Bella, F.; Nair, J. R. Super Soft All-Ethylene Oxide Polymer Electrolyte for Safe All-Solid Lithium Batteries. *Sci. Rep.* **2016**, *6*, 19892.
(10) Kim, G. T.; et al. UV cross-linked, lithium-conducting ternary polymer electrolytes containing ionic liquids. *J. Power Sources* **2010**, *195*, 6130−6137.
(11) Armand, M.; Endres, F.; MacFarlane, D. R.; Ohno, H.; Scrosati, B. Ionic-liquid materials for the electrochemical challenges of the future. *Nat. Mater.* **2009**, *8*, 621−629.
(12) Shin, J. Ionic liquids to the rescue? Overcoming the ionic conductivity limitations of polymer electrolytes. *Electrochem. Commun.* **2003**, *5*, 1016−1020.
(13) Falco, M. Understanding the Effect of UV-Induced Cross-Linking on the Physicochemical Properties of Highly Performing PEO/LiTFSI-Based Polymer Electrolytes. *Langmuir* **2019**, *35*, 8210.
(14) Motahari, F.; Raisi, A. Reducing the crystallinity of high molecular weight poly (ethylene oxide) using ultraviolet cross-linking for preparation of gas separation membranes. *J. Appl. Polym. Sci.* **2021**, *138*, 50059.
(15) Watanabe, M.; Nagano, S.; Sanui, K.; Ogata, N. Ionic Conductivity of Network Polymers from Poly(ethylene oxide) Containing Lithium Perchlorate. *Polym. J.* **1986**, *18*, 809−817.
(16) Joost, M.; et al. Ionic mobility in ternary polymer electrolytes for lithium-ion batteries. *Electrochim. Acta* **2012**, *86*, 330−338.
(17) Doytcheva, M.; et al. Ultraviolet-induced crosslinking of solid poly(ethylene oxide). *J. Appl. Polym. Sci.* **1997**, *64*, 2299−2307.
(18) Di Lecce, D.; Sharova, V.; Jeong, S.; Moretti, A.; Passerini, S. A multiple electrolyte concept for lithium-metal batteries. *Solid State Ion.* **2018**, *316*, 66−74.
(19) Gerbaldi, C.; et al. UV-cured polymer electrolytes encompassing hydrophobic room temperature ionic liquid for lithium batteries. *J. Power Sources* **2010**, *195*, 1706−1713.
(20) Nair, J. R.; et al. UV-cured methacrylic membranes as novel gel−polymer electrolyte for Li-ion batteries. *J. Power Sources* **2008**, *178*, 751−757.
(21) Yoshida, K.; et al. Oxidative-Stability Enhancement and Charge Transport Mechanism in Glyme−Lithium Salt Equimolar Complexes. *J. Am. Chem. Soc.* **2011**, *133*, 13121−13129.
(22) Wang, J.; et al. Superconcentrated electrolytes for a high-voltage lithium-ion battery. *Nat. Commun.* **2016**, *7*, 12032.
(23) Suo, L.; et al. Water-in-salt" electrolyte enables high-voltage aqueous lithium-ion chemistries. *Science* **2015**, *350*, 938−943.
(24) Gao, X.; Wu, F.; Mariani, A.; Passerini, S. Concentrated Ionic-Liquid-Based Electrolytes for High-Voltage Lithium Batteries with Improved Performance at Room Temperature. *ChemSusChem* **2019**, *12*, 4185−4193.
(25) Chen, F.; Howlett, P.; Forsyth, M. Na-Ion Solvation and High Transference Number in Superconcentrated Ionic Liquid Electrolytes: A Theoretical Approach. *J. Phys. Chem. C* **2018**, *122*, 105−114.
(26) Chen, C.-Y.; et al. Ionic liquid electrolytes with high sodium ion fraction for high-rate and long-life sodium secondary batteries. *J. Power Sources* **2016**, *332*, 51−59.
(27) Giffin, G. A.; Moretti, A.; Jeong, S.; Passerini, S. Decoupling effective Li+ ion conductivity from electrolyte viscosity for improved room-temperature cell performance. *J. Power Sources* **2017**, *342*, 335−341.
(28) Pal, U.; et al. Enhanced ion transport in an ether aided super concentrated ionic liquid electrolyte for long-life practical lithium metal battery applications. *J. Mater. Chem. A* **2020**, *8*, 18826−18839.
(29) Pal, U.; et al. Improved Li-Ion Transport by DME Chelation in a Novel Ionic Liquid-Based Hybrid Electrolyte for Li−S Battery Application. *J. Phys. Chem. C* **2018**, *122*, 14373−14382.
(30) Pal, U.; et al. Interphase control for high performance lithium metal batteries using ether aided ionic liquid electrolyte. *Energy Environ. Sci.* **2022**, *15*, 1907−1919.
(31) Pal, U.; et al. Developing a High-Performing Spinel $LiMn_2O_4$ Cathode Material with Unique Morphology, Fast Cycling and Scaled Manufacture. *Batteries Supercaps* **2024**, *7*, e202400072.
(32) He, R.; Kyu, T. Effect of Plasticization on Ionic Conductivity Enhancement in Relation to Glass Transition Temperature of Crosslinked Polymer Electrolyte Membranes. *Macromolecules* **2016**, *49*, 5637−5648.
(33) Zhang, M.; et al. Advanced High-Voltage Electrolyte Design Using Poly(ethylene oxide) and High-Concentration Ionic Liquids for All-Solid-State Lithium Metal Batteries. *ACS Appl. Mater. Interfaces* **2024**, *16*, 56095−56105.
(34) Al-Masri, D.; Yunis, R.; Hollenkamp, A. F.; Pringle, J. M. Designing Solid-State Electrolytes through the Structural Modification of a High-Performing Ionic Liquid. *ChemElectroChem.* **2020**, *7*, 4118−4123.
(35) Jin, L.; et al. Structure and Transport Properties of a Plastic Crystal Ion Conductor: Diethyl(methyl)(isobutyl)phosphonium Hexafluorophosphate. *J. Am. Chem. Soc.* **2012**, *134*, 9688−9697.
(36) Susan, Md. A. B. H.; Kaneko, T.; Noda, A.; Watanabe, M. Ion Gels Prepared by in Situ Radical Polymerization of Vinyl Monomers in an Ionic Liquid and Their Characterization as Polymer Electrolytes. *J. Am. Chem. Soc.* **2005**, *127*, 4976−4983.
(37) Joost, M.; Kim, G. T.; Winter, M.; Passerini, S. Phase stability of Li-ion conductive, ternary solid polymer electrolytes. *Electrochim. Acta* **2013**, *113*, 181−185.
(38) Berthier, C.; Gorecki, W.; Minier, M.; Armand, M. B.; Chabagno, J. M.; Rigaud, P. Microscopic Investigation of Ionic Conductivity in Alkali Metal Salts-Poly(Ethylene Oxide) Adducts. *Solid State Ionics* **1983**, *11*, 91−95.
(39) Stettner, T.; Lingua, G.; Falco, M.; Balducci, A.; Gerbaldi, C. Protic Ionic Liquids-Based Crosslinked Polymer Electrolytes: A New Class of Solid Electrolytes for Energy Storage Devices. *Energy Technol.* **2020**, *8*, 2000742.
(40) Kimura, K.; Motomatsu, J.; Tominaga, Y. Correlation between Solvation Structure and Ion-Conductive Behavior of Concentrated Poly(ethylene carbonate)-Based Electrolytes. *J. Phys. Chem. C* **2016**, *120*, 12385−12391.
(41) Nguyen, H. T. T.; et al. Facile Li^+ Transport in Interpenetrating O- and F-Containing Polymer Networks for Solid-State Lithium Batteries. *Adv. Funct. Mater.* **2023**, *33*, 2213469.
(42) Xu, K.; Ding, S. P.; Jow, T. R. Toward Reliable Values of Electrochemical Stability Limits for Electrolytes. *J. Electrochem. Soc.* **1999**, *146*, 4172−4178.
(43) Herbers, L.; et al. The Influence of Polyethylene Oxide Degradation in Polymer-Based Electrolytes for NMC and Lithium Metal Batteries. *Adv. Energy Sustain. Res.* **2023**, *4*, 2300153.

https://doi.org/10.1021/acsapm.4c02520
ACS Appl. Polym. Mater. 2024, 6, 14469−14476